Progress Report

Kotora Sasaki

About me

佐々木 誇虎 （Kotora Sasaki）

from Sapporo, Hokkaido

University of Tsukuba
College of Physics
→ Doctoral Program in Physics (First-year PhD)

Hobbies: Music !!!!!!!!!!!!!!!! (and many others)

1. Introduction

Massive star and molecular cloud

Massive stars ($> 8\ M_\odot$)
key drivers of ISM/Galaxy evolution (via UV, feedback)
Formation mechanism remains an open question.

Key observational environments

- filament structures
- hub-filament systems (HFSs):
  mass convergence via filaments
- cloud-cloud collisions (CCCs):
  rapid gas compression

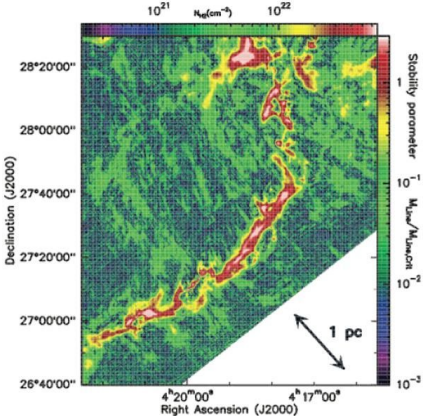

Taurus B211+L1495 (Palmeirim et al. 2013)

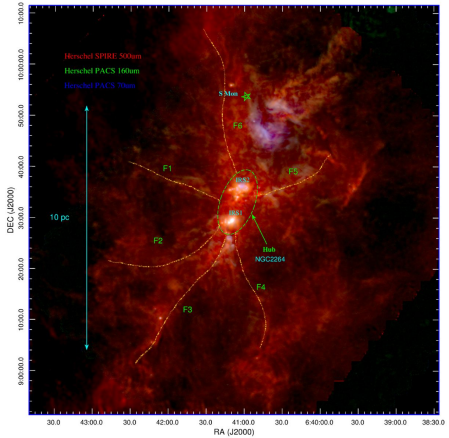

NGC2264 (based on Kumar et al. 2020)

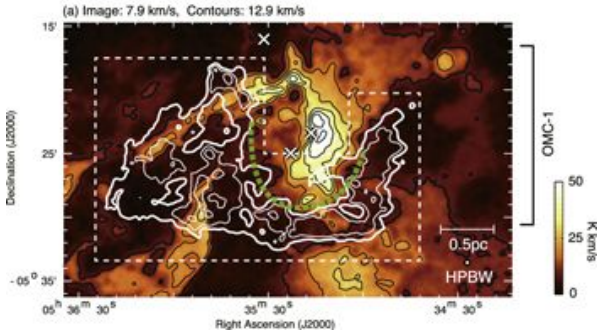

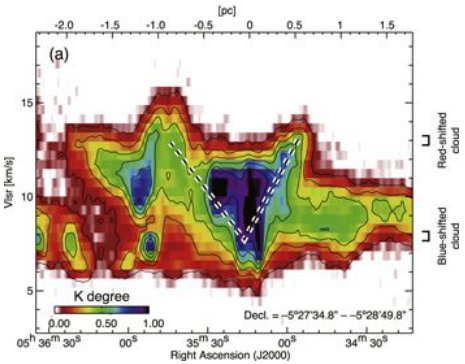

OMC-1 (based on Fukui et al. 2018a)

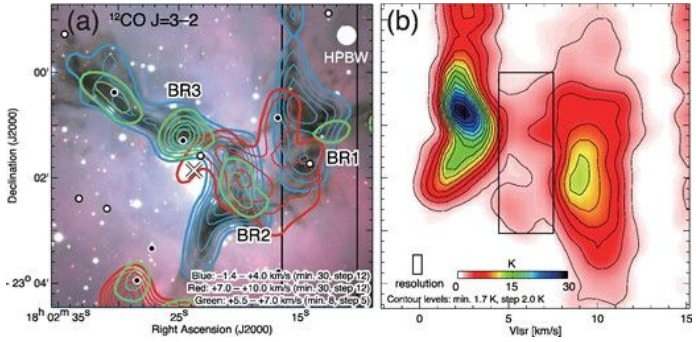

M20 (Fukui et al. 2021)

1. Introduction

Global hierarchical collapse (GHC)

Global hierarchical collapse
(GHC, e.g., V´azquez-Semadeni et al. 2019）

a mass cascade driven by gravity-driven, multi-scale converging flows

smaller dense structures actively accrete mass from their larger parent structures

Unified observational manifestations

- filament fragmentation: anisotropic mass accretion within filaments
- hub-filament systems (HFS): mass convergence into central hubs
- cloud-cloud collisions (CCC): localized versions of converging flows

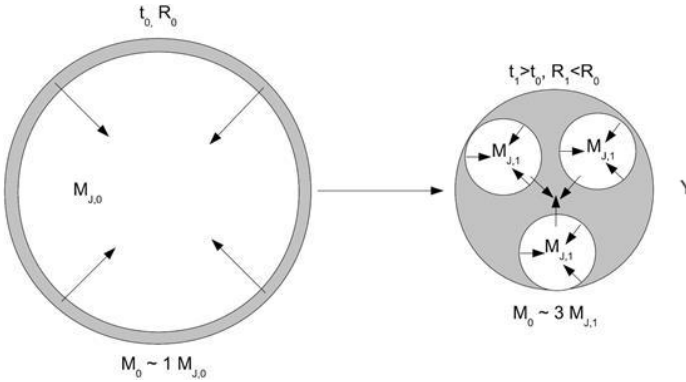

V´azquez-Semadeni et al. 2019

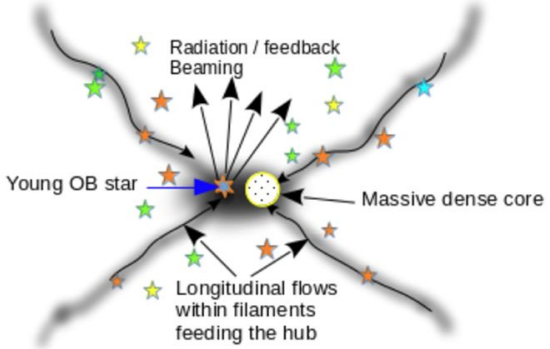

Based on Kumar et al. 2020

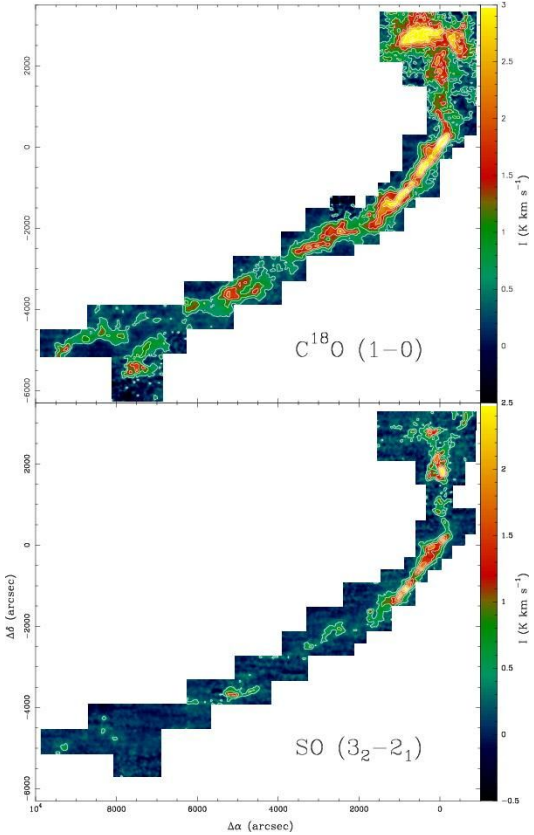

Taurus B211+L1495（Hacar et al. 2013）

1. Introduction

Previous studies using dendrogram

Dendrogram algorithm（Rosolowsky et al. 2008）
identifies hierarchical structures in 3D data cubes
based on emission intensity

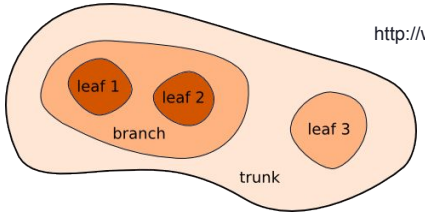

http://www.dendrograms.org/

・Maddalena GMC (Shen et al. 2024)
comparision of physical properties between hierarchical and monolithic structures
・Rosette molecular cloud (He et al. 2026)
global structure supports the GHC model.

Previous studies are:
・limited to single case studies.
・limited to verifying scaling laws.
= not verified the relationship between the hierarchical structure actually extracted by the dendrogram and the observed phenomena.

A more comprehensive approach is needed, including verification of the relationship with observational phenomena and statistical investigation of physical quantities.

All based on Shen et al. 2024

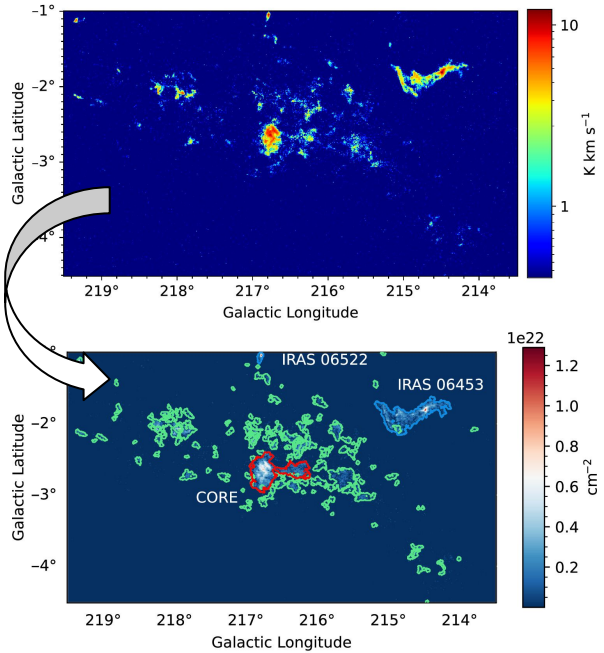

1. Introduction

Aims

Main goal: systematically evaluate the relationship between hierarchical structures and star formation activity across multiple molecular clouds in the Galaxy

- data: FUGIN project (Nobeyama 45m telescope; Umemoto et al. 2017)
- algorithm: apply dendrogram (Rosolowsky et al. 2008) to extract hierarchical structures
- discuss formation and evolutionary processes based on physical properties derived from these structures

FUGIN data

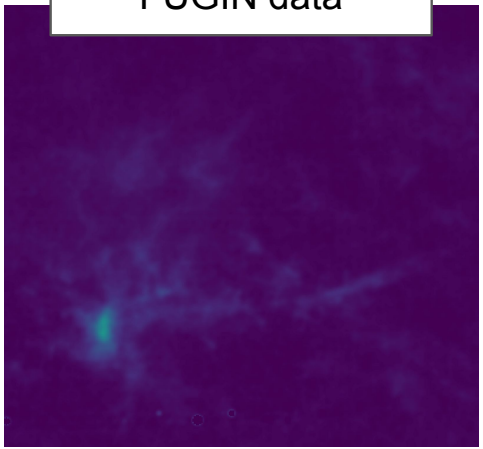

structure extraction via dendrogram

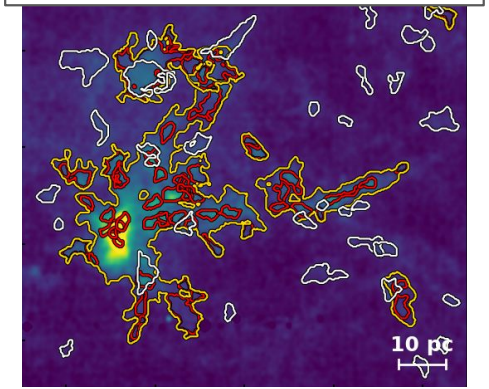

calculation of physical properties & discussion

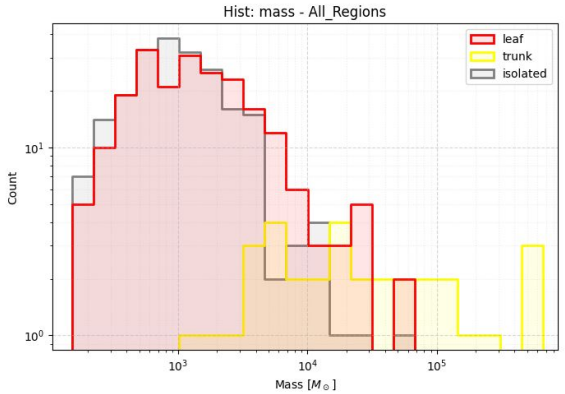

2. Data

FUGIN

FUGIN Project

（FOREST Unbiased Galactic plane Imaging survey with the Nobeyama 45m telescope, Umemoto et al. 2017）

large-scale simultaneous survey of CO isotopologues in the Galactic plane

high angular resolution: ~ 20", velocity resolution: 1.3 km s^{-1}

Target line: ^{13}CO(J = 1-0)（**optically thin tracer suitable for probing internal cloud structures**）

Target regions: selected 13 candidate regions for fragmented filaments / HFSs / CCCs analysis

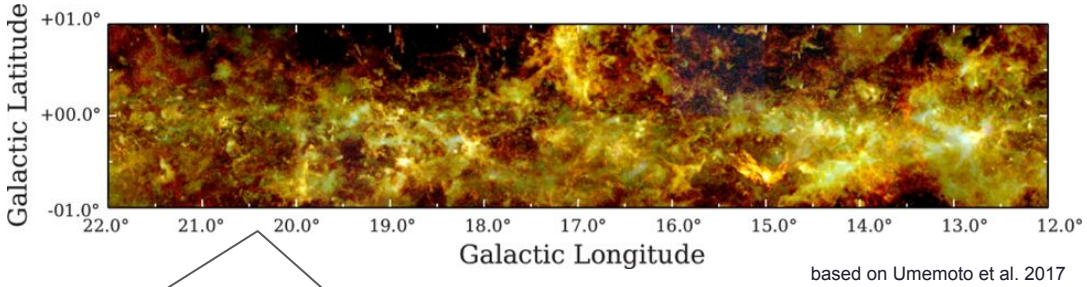

based on Umemoto et al. 2017

three-color composite image of ^{12}CO, ^{13}CO, C^{18}O(J = 1-0)

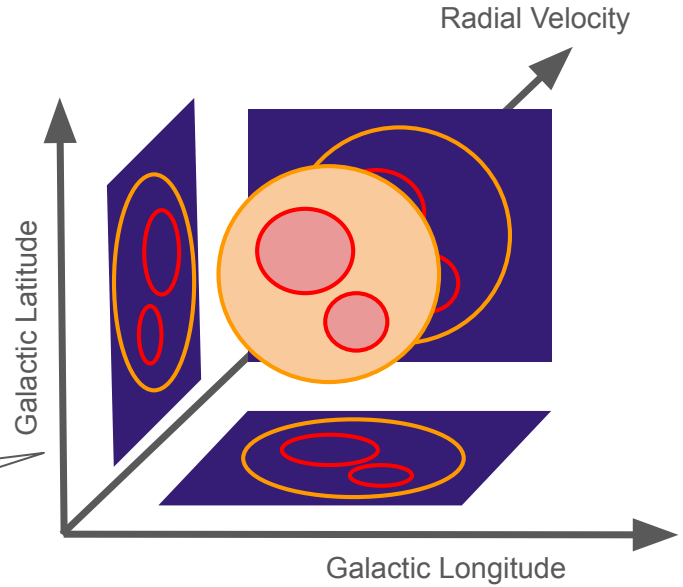

extraction of 3D hierarchical structures from the (*l, b, v*) data cube
visualization via projection onto 2D planes

2. Data

SPICY YSO catalog, Hi-GAL clump catalog

SPICY catalog (Spitzer / IRAC)

comprehensive list of mid-IR identified young stellar object (YSO) candidates (Kuhn et al. 2021)
retained only Class I and II YSOs to focus on active early stages
evolutionary scheme applies primarily to low-mass YSO
→ **analysis is explicitly restricted to tracing the early stages of low-mass star formation.**

Hi-GAL catalog (Herschel)

physical property catalog of dense clumps (Elia et al. 2017, 2021)
to evaluate early stages of high-mass star formation (Motte et al. 2018), resolving ~ 0.5 pc (**protoclusters**)

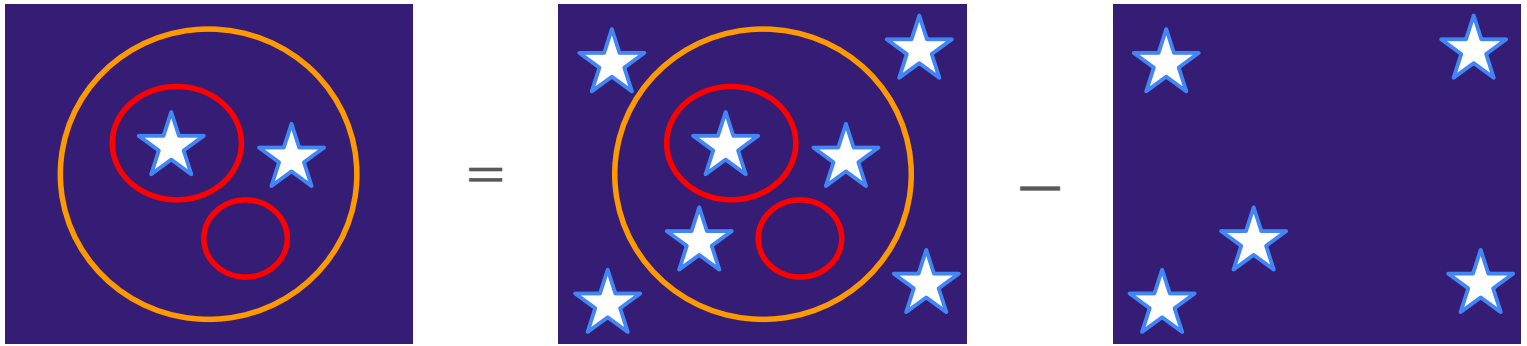

$$N_{\rm true} = N_{\rm in} - S_{\rm in}\Sigma_{\rm out} = N_{\rm in} - S_{\rm in}\frac{N_{\rm out}}{S_{\rm out}}$$

3. Method

Dendrogram and physical properties

Dendrogram algorithm（Rosolowsky et al. 2008）
identifies hierarchical structures in 3D data cubes
based on emission intensity

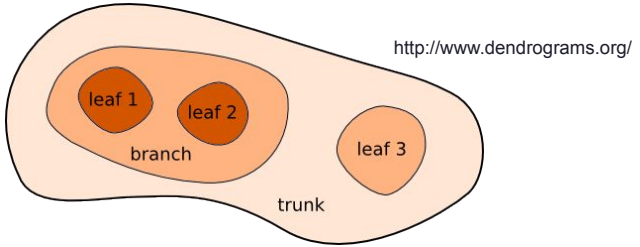

- leaf: smallest unit with no substurcture
- branch: structure containing substurctures
- trunk: top-level structure (largest scale)
- isolated: single structure with no parent or child (used for comparison)

$\mu = 2.8$ mean molecular weight
$m_{\rm H}$ mass of hyudorgen atom
$A_{\rm pix}$ physical area of one pixel

Derivation of physical properties

- effective radius (R) Derived from projected area (S) $R = \sqrt{S/\pi}$
- mass (M) derived from H_2 column density (N_{H_2}) assuming LTE ($M = \mu m_{\rm H} A_{\rm pix} \sum N_{\rm H_2}$)
- volume density (ρ) assumed spherical symmetry ($\rho = \frac{M}{V}$ $V = \frac{4}{3}\pi R^3$)
- virial parameter ($\alpha_{\rm vir}$) derived from velocity dispersion (σ_v) $\alpha_{\rm vir} = \frac{5\sigma_v^2 R}{GM}$

evaluate the balance between gravity and turbulence (Bertoldi & McKee 1992)

3. Method

Core algorithm of dendrogram

leaf detection from local maximums

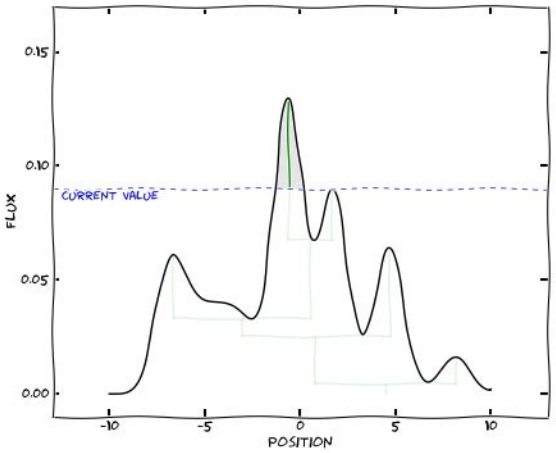

merging two local maxima into a branch

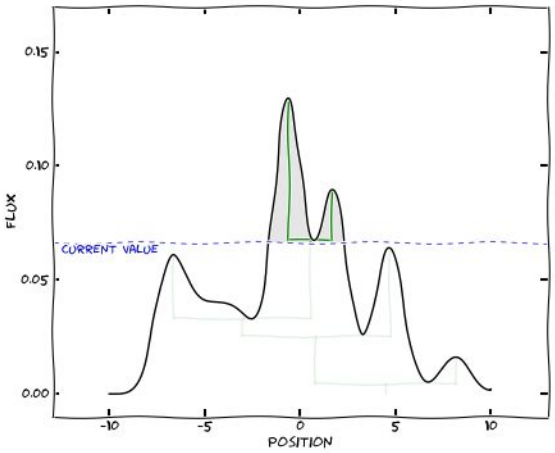

hierarchical formation

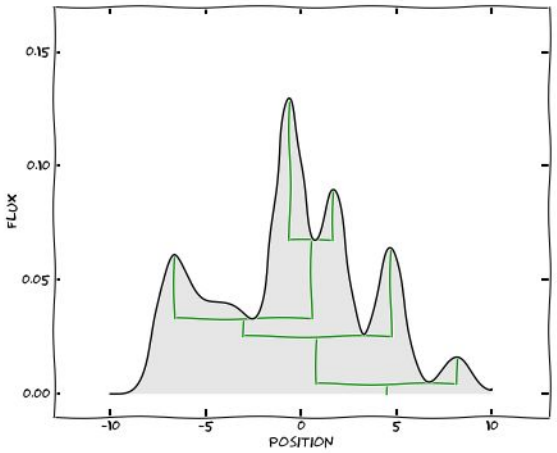

http://www.dendrograms.org/

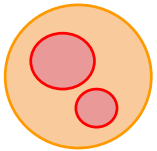

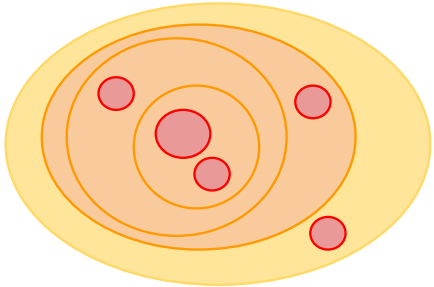

3. Method

Parameter of dendrogram

- min_value

  the minimum intensity (threshold) to extract as a structure

  To prevent the structure from being truncated at the edge of the data, it is set to the 99.9th percentile value of the PPV data boundary.

- min_delta

  the minimum height (luminance difference) of the structure

  It is set to 1σ to eliminate false peaks caused by noise.

- min_npix

  minimum area size acceptable as a structure

$$\left(\frac{1.5\theta}{8.5}\right)^2 \times 2$$

represents velocity range
2 × 0.65 [km s^{-1} / pix] = 1.3 [km s^{-1}]

θ = angular resolution [arcsec]
8.5 = pixel size [arcsec / pix]
following Shen et al. (2024)

http://www.dendrograms.org/

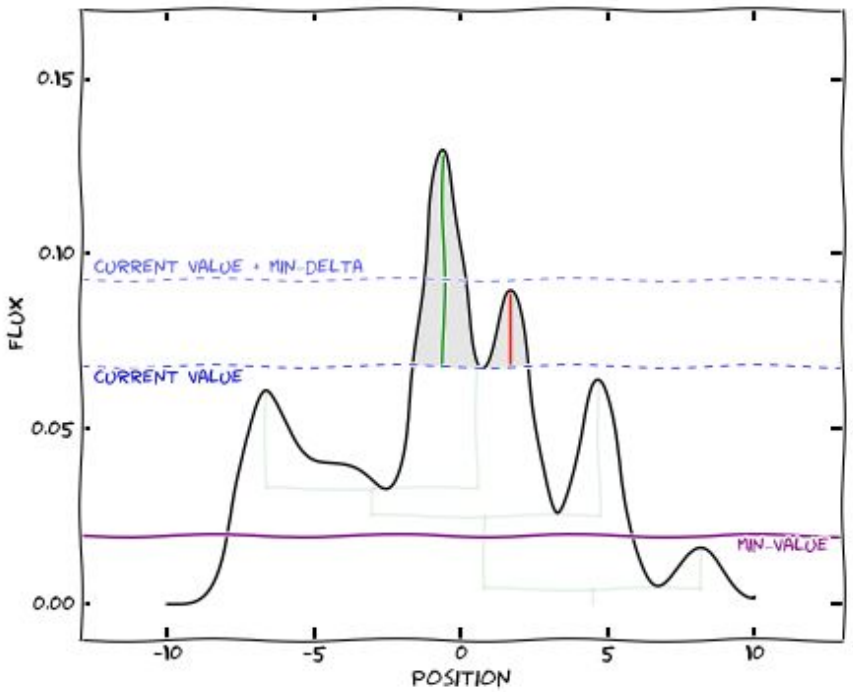

4. Results

Analysis results of W33 / N14

W33: tracing HFS and kinematics

- leaves: dense gas in central hub and along filaments (indicating fragmentation)
- trunks: overall system tracing radial filaments
- distinct velocity gradients along filaments toward hub

N14: tracing oscillatory velocity patterns

- leaves: individual dense gas clumps at velocity peaks
- trunks: broader gas exhibiting global oscillating motion

based on Liu et al. 2021

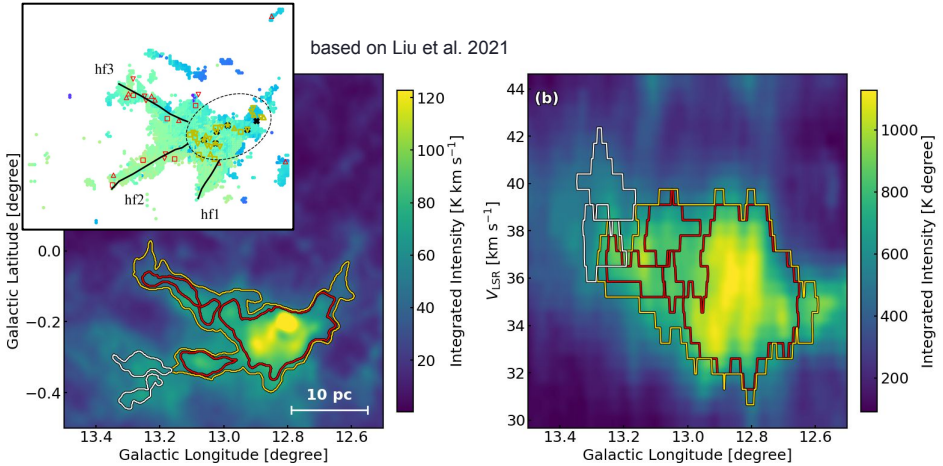

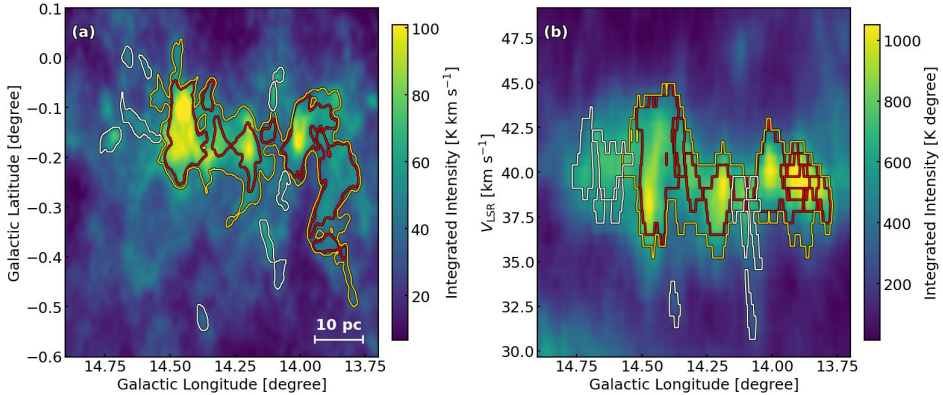

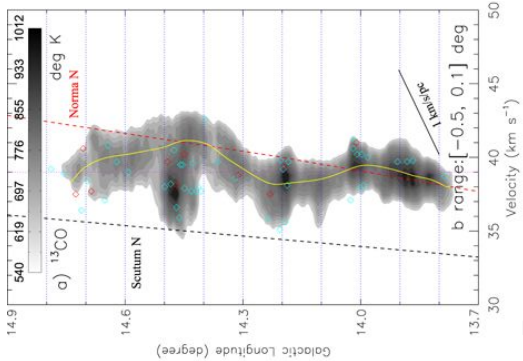

based on Dewangan et al. 2020

4. Results

Analysis results of W33 / N14

W33: tracing HFS and kinematics

- leaves: dense gas in central hub and along filaments (indicating fragmentation)
- trunks: overall system tracing radial filaments
- distinct velocity gradients along filaments toward hub

N14: tracing oscillatory velocity patterns

- leaves: individual dense gas clumps at velocity peaks
- trunks: broader gas exhibiting global oscillating motion

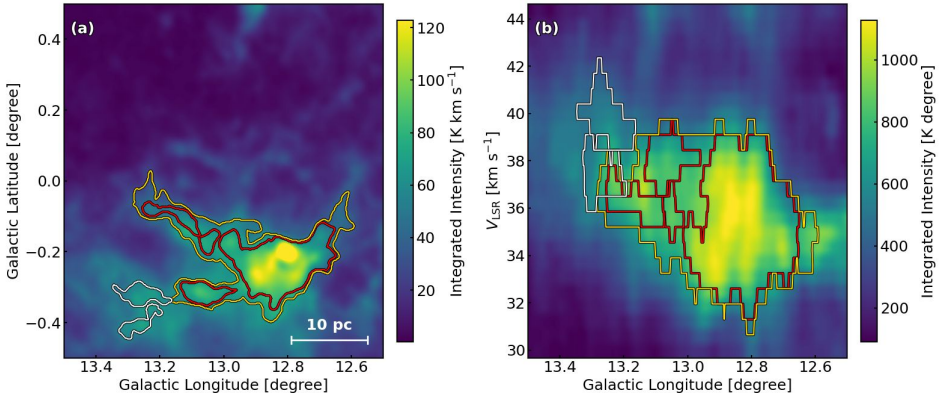

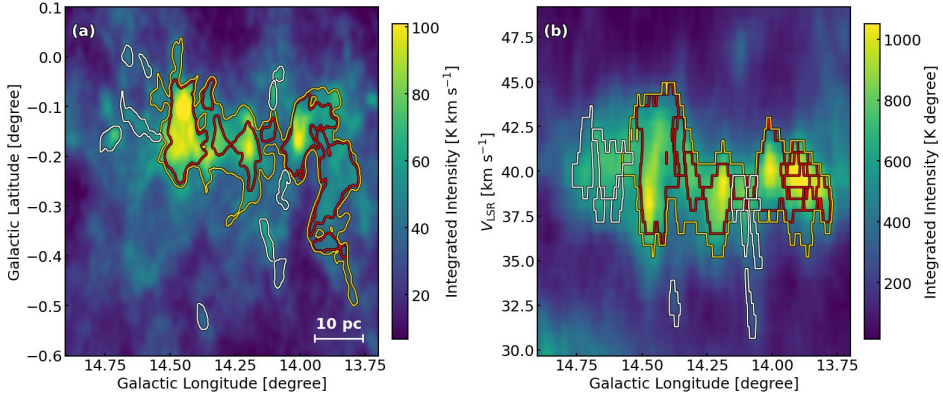

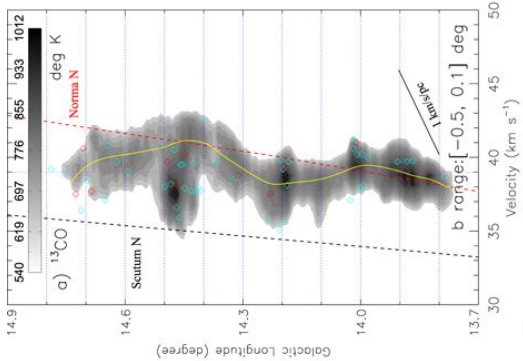

based on Dewangan et al. 2020

4. Results

Analysis results of N35 / W51

N35: tracing CCC and kinematics

- leaves: denser gas concentrations formed by the collision
- trunks: two distinct structures along the gradient
- hierarchies distributed precisely along the steep velocity gradient

W51: tracing CCC and kinematics

- leaves: distributed across distinct velocity components
- trunks: span multiple components and connecting bridge

based on Torii et al. 2018

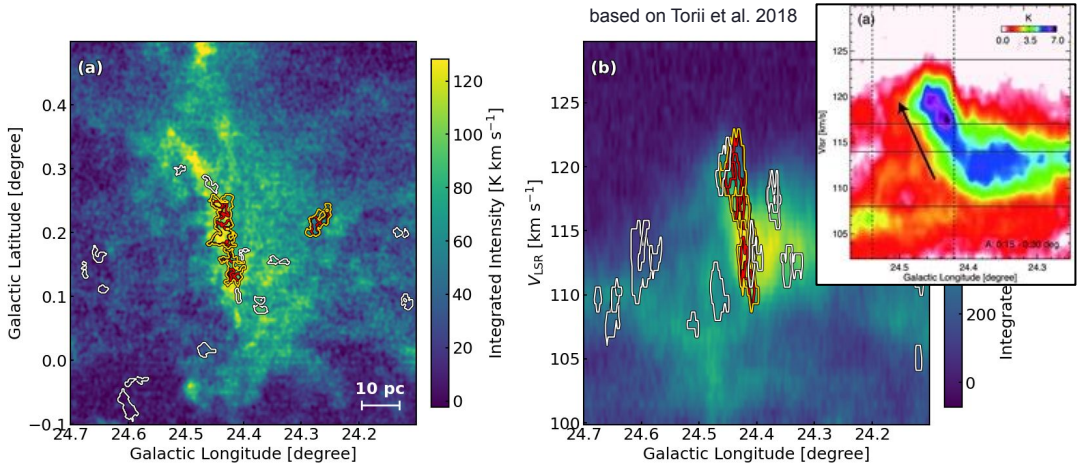

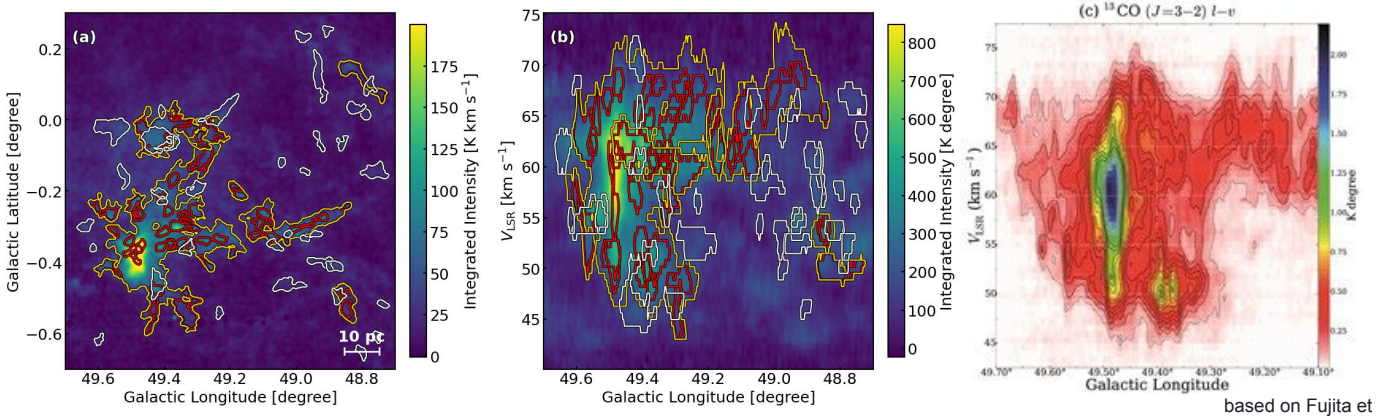

based on Fujita et al. 2021

4. Results

Analysis results of N35 / W51

N35: tracing CCC and kinematics

- leaves: denser gas concentrations formed by the collision
- trunks: two distinct structures along the gradient
- hierarchies distributed precisely along the steep velocity gradient

W51: tracing CCC and kinematics

- leaves: distributed across distinct velocity components
- trunks: span multiple components and connecting bridge

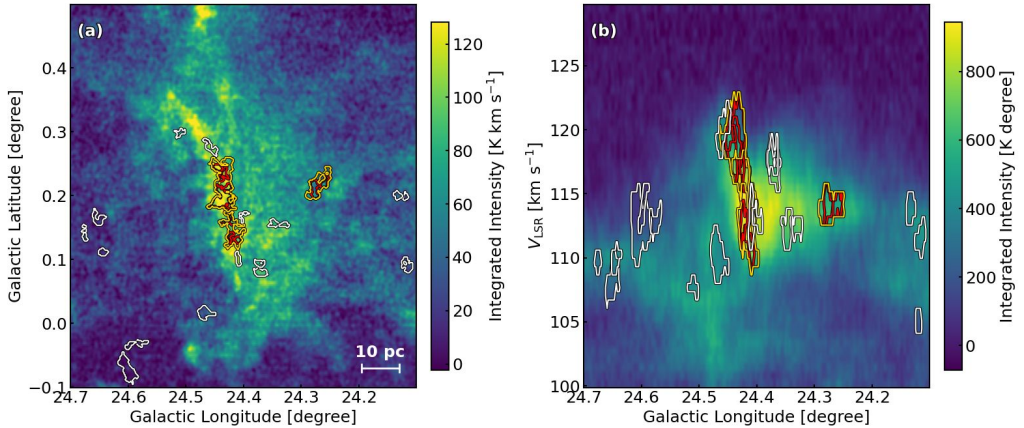

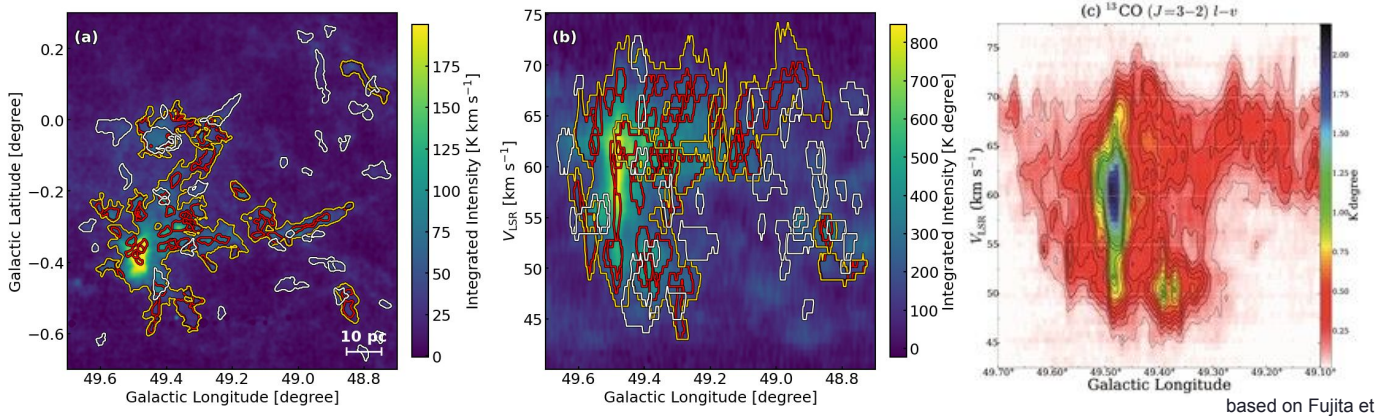

based on Fujita et al. 2021

4. Results

Histogram of physical properties of the entire structure

The overall distributions of these properties exhibit substantial overlap.

This region-to-region variance obscures the intrinsic differences between the structural categories, making visual distinction challenging.

We performed a Type II analysis of variance (ANOVA).

$$y = \mu + \alpha_{\text{region}} + \beta_{\text{structure}} + \epsilon$$

$$\Rightarrow y_{\text{adj}} = y - \alpha_{\text{region}}$$

$$= \mu + \beta_{\text{structure}} + \epsilon$$

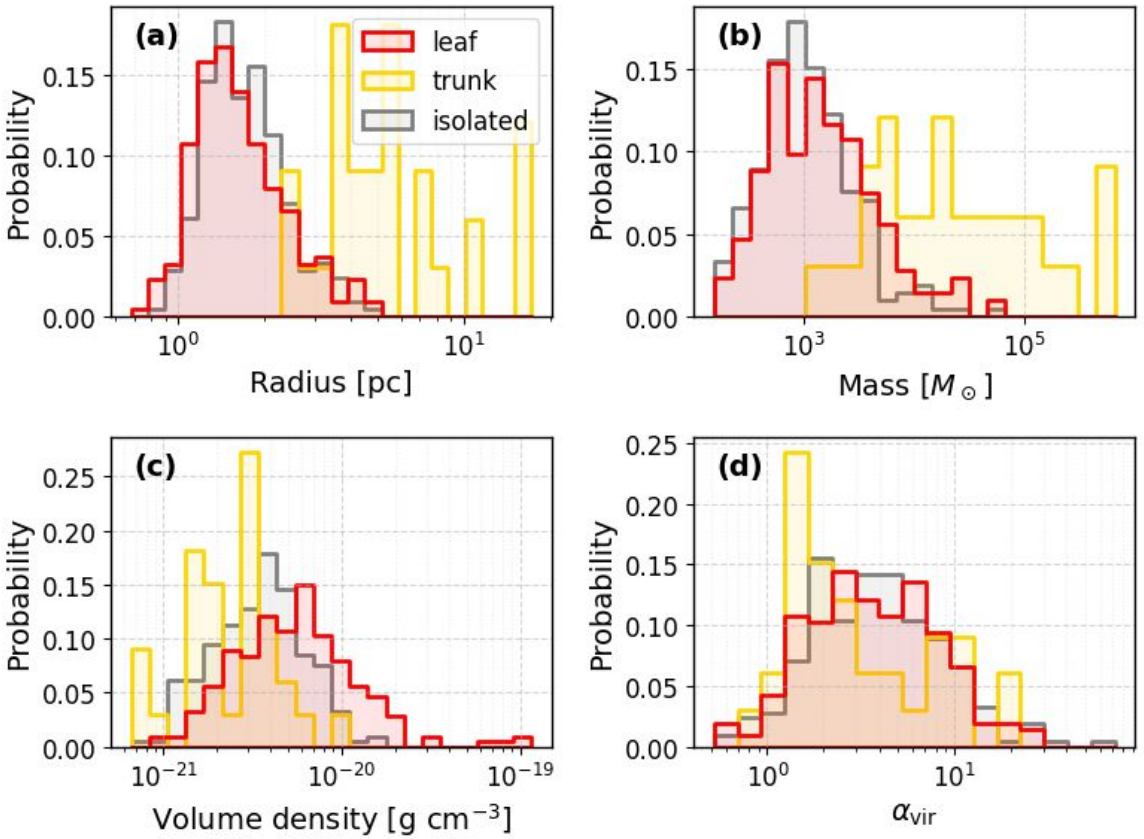

4. Results

Adjusted physical properties (trunk vs. isolated)

radius, mass: **trunk > isolated**
virial parameter: **trunk < isolated**

→ **Large-scale, massive environments are physically required to harbor internal hierarchical structures.**

volume density: **trunk < isolated**

- isolated structures:
  trace independent high-density regions without extended envelopes
- trunks:
  encompass both internal high-density structures and their surrounding low-density extended gas

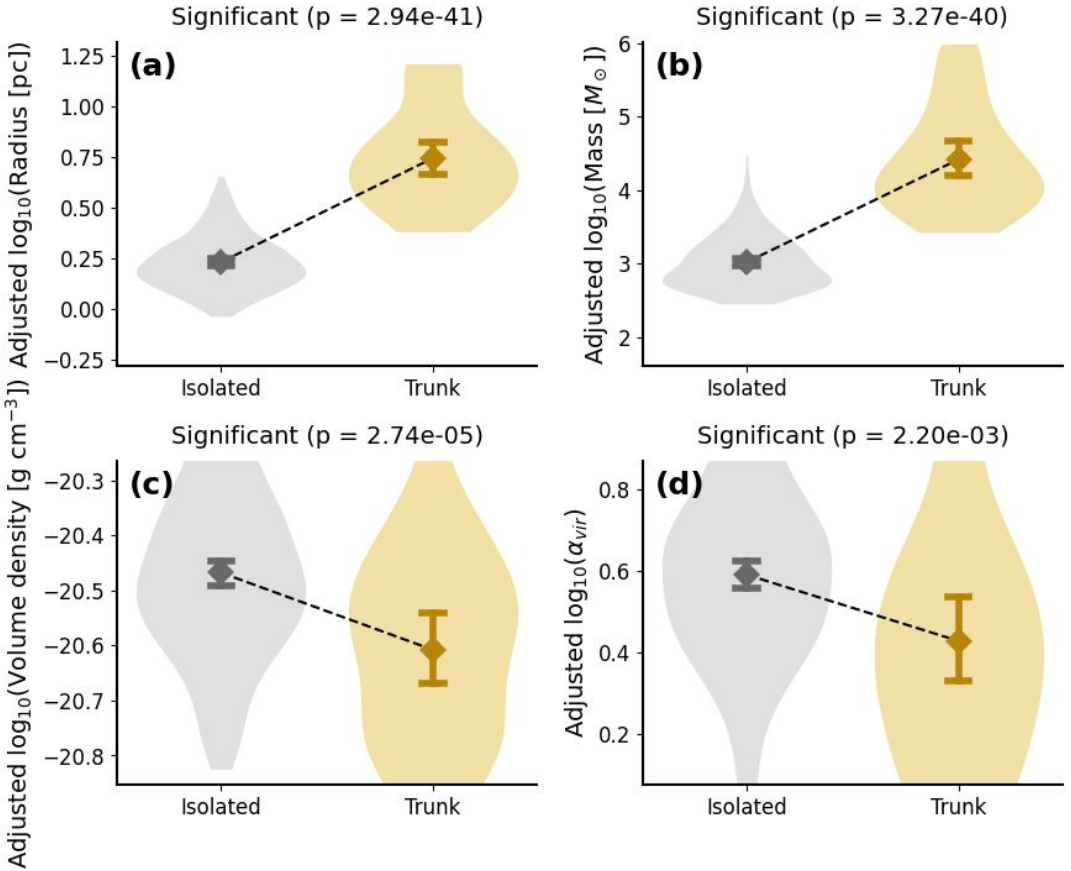

4. Results

Adjusted physical properties (leaf vs. isolated)

radius: no significant difference
mass, volume density: **leaf > isolated**
virial parameter: **leaf < isolated**

→ **Internal structures (Leaves) acquires more gas through physical processes stemming from the existence of the hierarchy, and as a result provide a more favorable environment for star formation compared to isolated structures.**

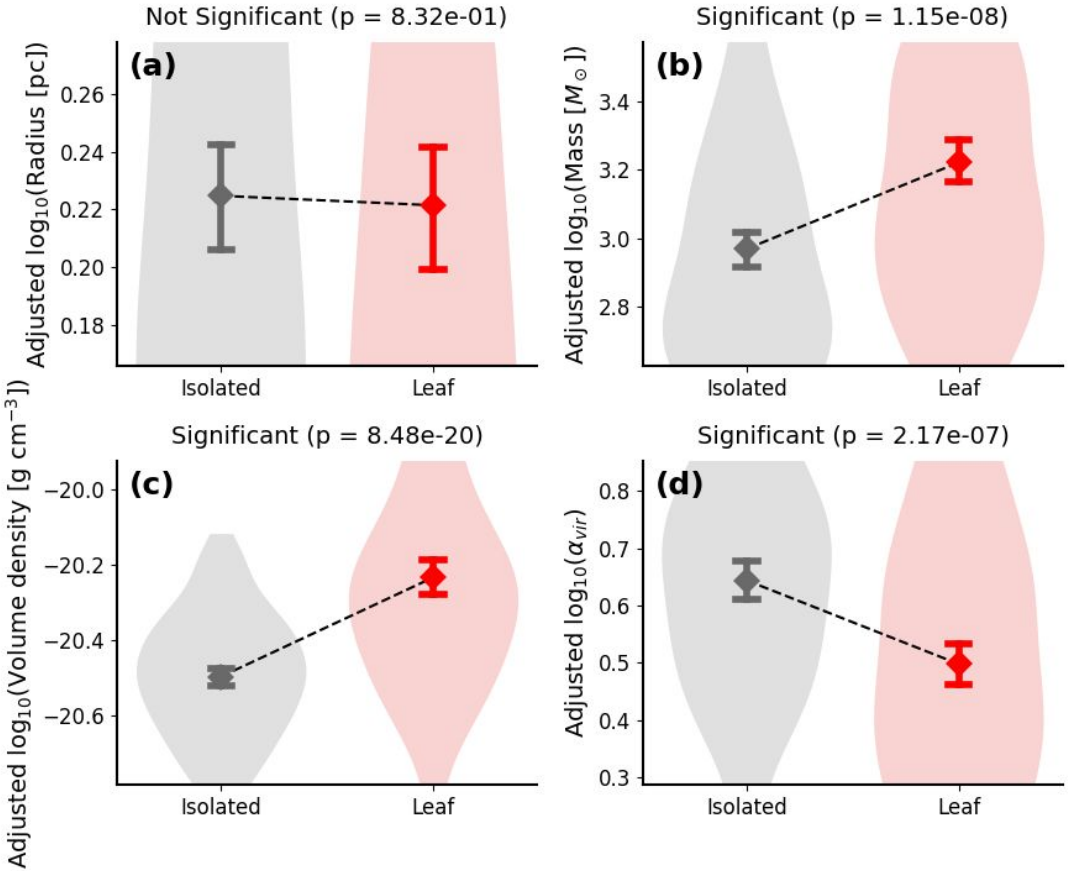

4. Results

Compare with YSO (low-mass star precursor)

adjusted number: not significant

association probability:
within each other's margin of error

mean number:
within each other's margin of error

Low-mass star formation activity exhibit no significant dependence on the hierarchical nature of the host structure.

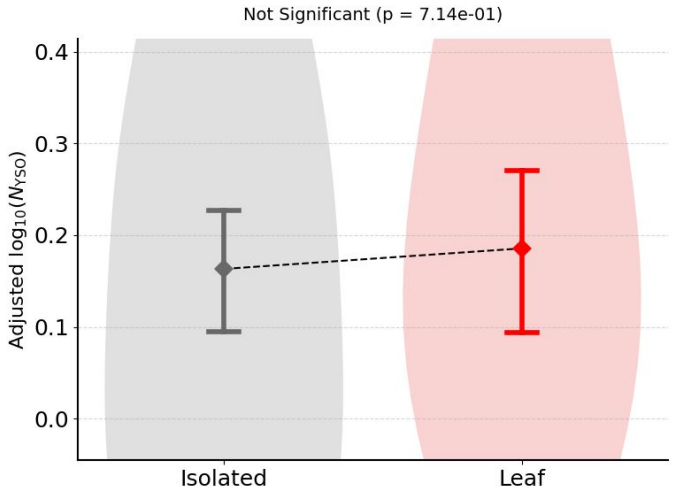

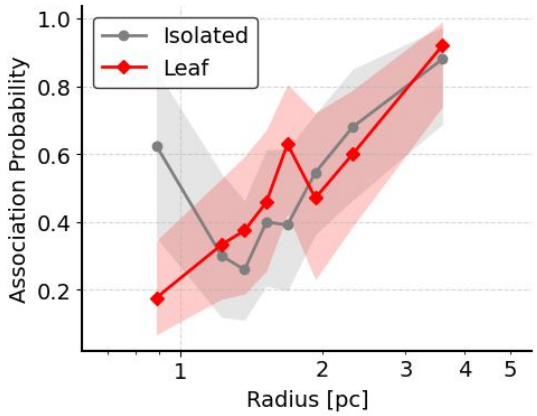

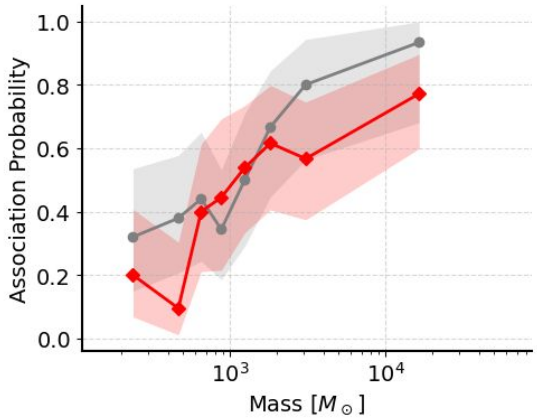

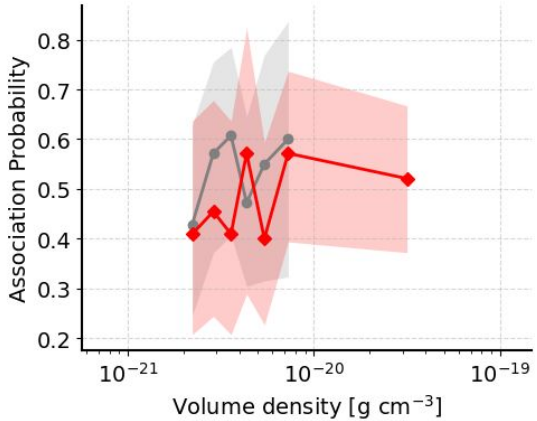

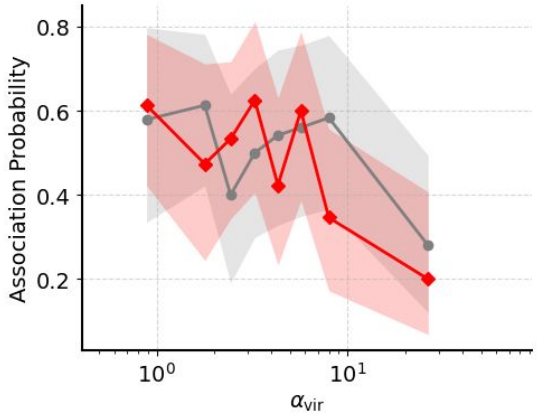

4. Results

Compare with YSO (low-mass star precursor)

adjusted number: not significant

association probability:
within each other's margin of error

mean number:
within each other's margin of error

Low-mass star formation activity exhibit no significant dependence on the hierarchical nature of the host structure.

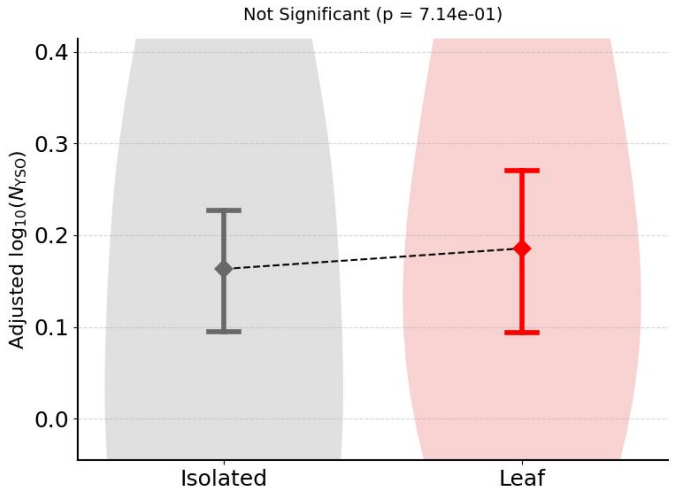

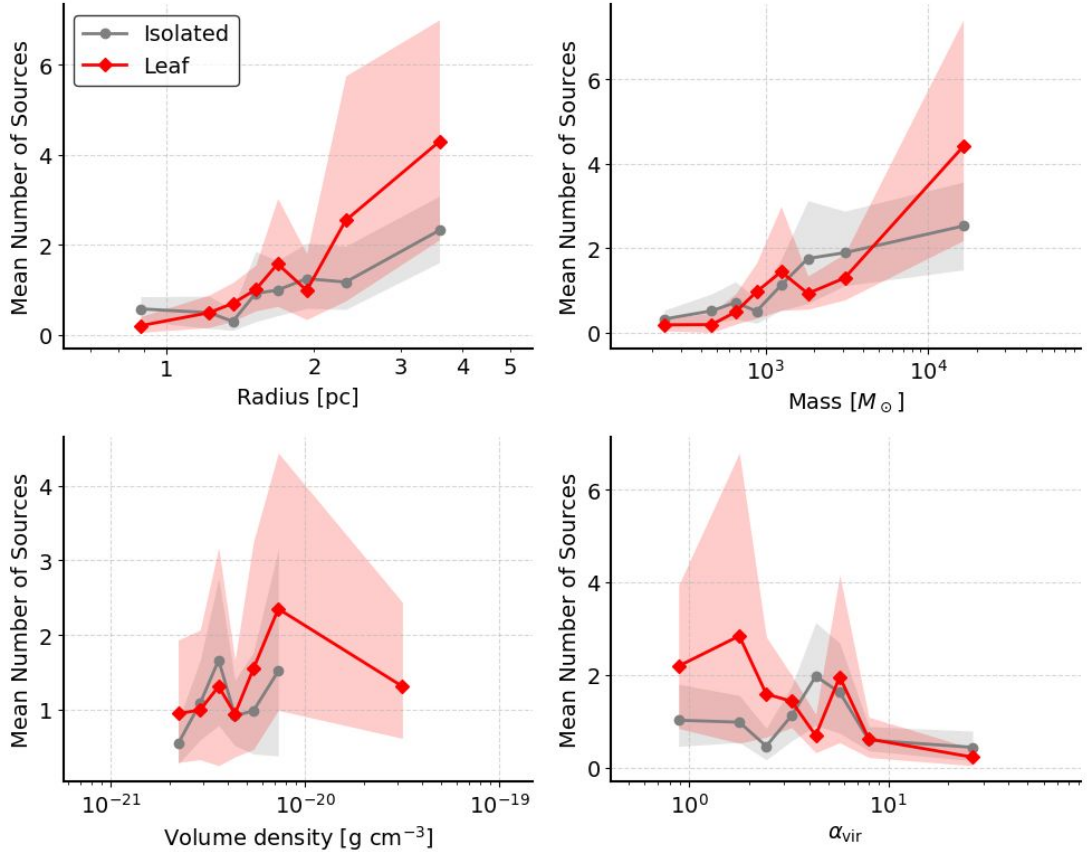

4. Results

Compare with Hi-GAL clump (high-mass star precursor)

adjusted Number: **leaf > isolated**

association probability:
within each other's margin of error

mean number: **leaf > isolated**
at the largest radii, mass, lowest virial prameter

Leaves retain the same amount of gas even after having actively consumed a larger amount of gas to form high-mass clumps.

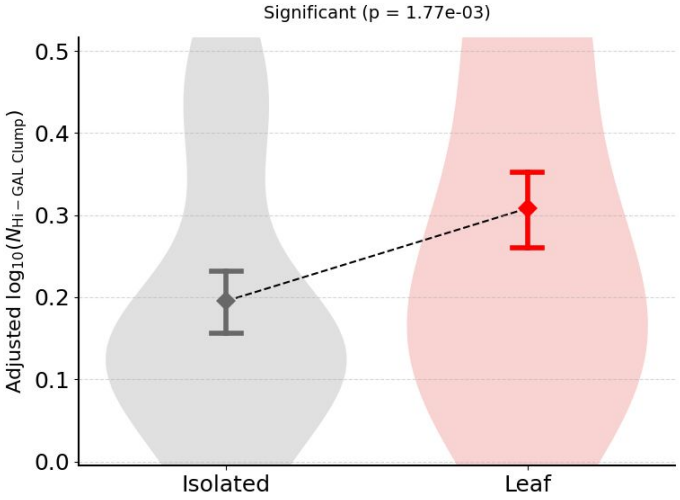

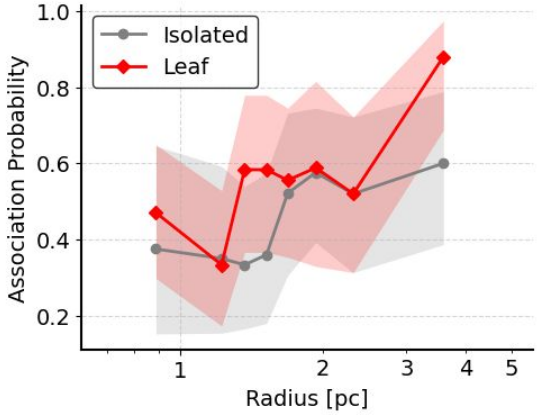

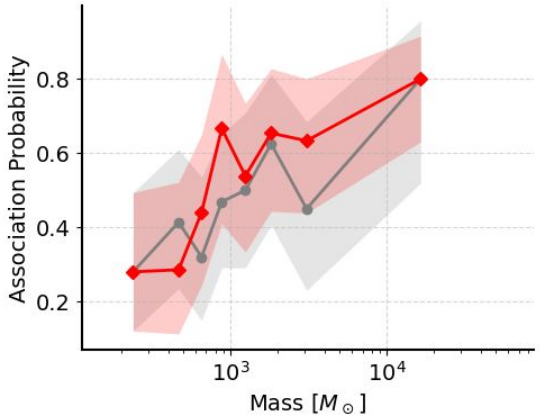

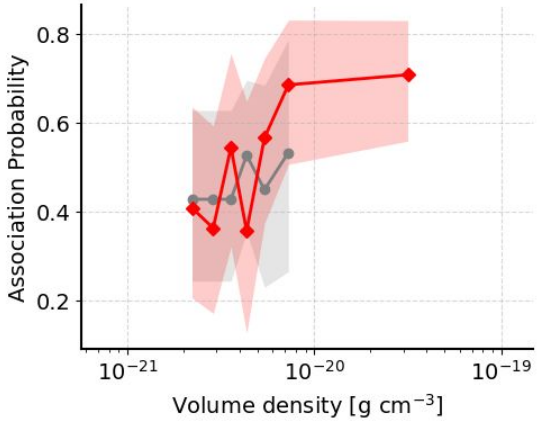

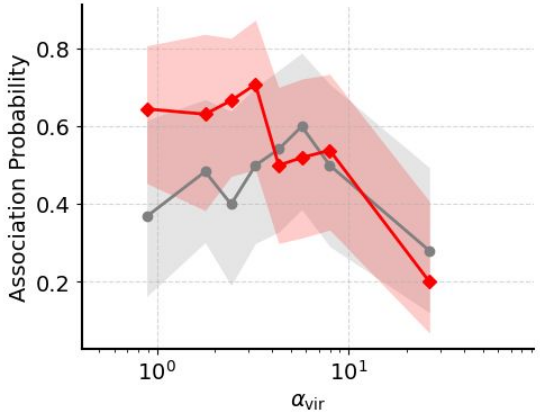

4. Results

Compare with Hi-GAL clump (high-mass star precursor)

adjusted Number: **leaf > isolated**

association probability:
within each other's margin of error

mean number: **leaf > isolated**
at the largest radii, mass, lowest virial prameter

Leaves retain the same amount of gas even after having actively consumed a larger amount of gas to form high-mass clumps.

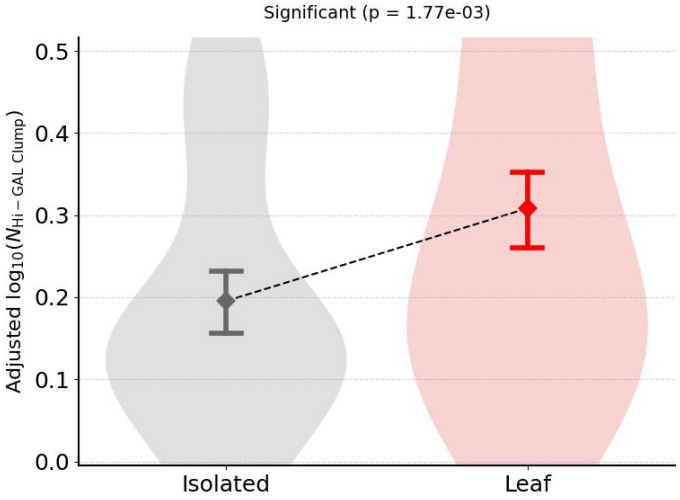

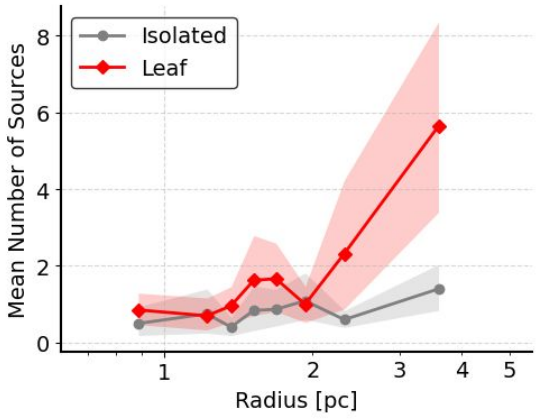

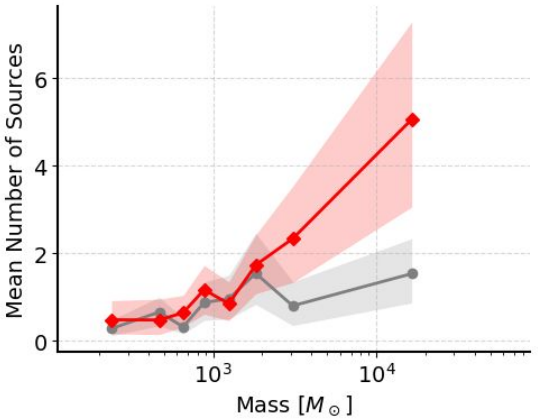

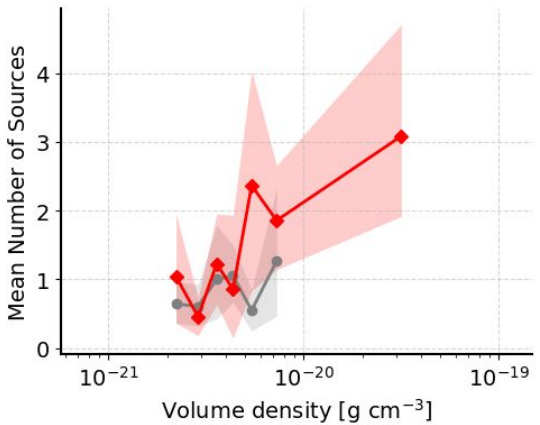

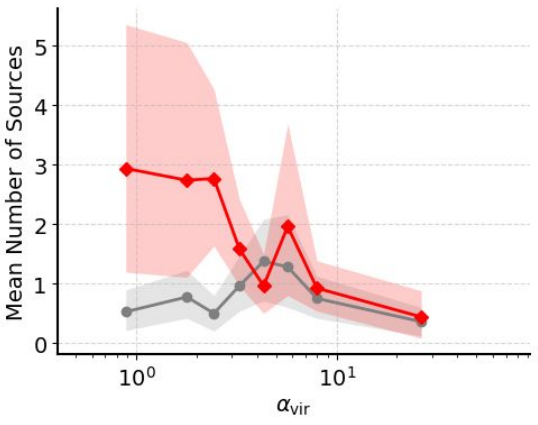

5. Discussion

Hierarchical mass accumulation

・trunk

formed by events driven by converging flow
(e.g., gas accretion onto filaments, CCC)

grows to a large size and high mass, and acquires strong self-gravity

a reservoir that continuously collects gas from its surroundings due to its deep gravitational potential

・leaf

formed by the fragmentation of the trunk

high mass growth due to continuous gas accretion from the trunk, and high-frequency interactions due to trunk confinement
(e.g., gas accretion to the hub at HFS, scattering across multiple velocity components in a bridge structure)

a site where gas accretion and interaction allow for continuous growth and star formation without depleting the gas supply

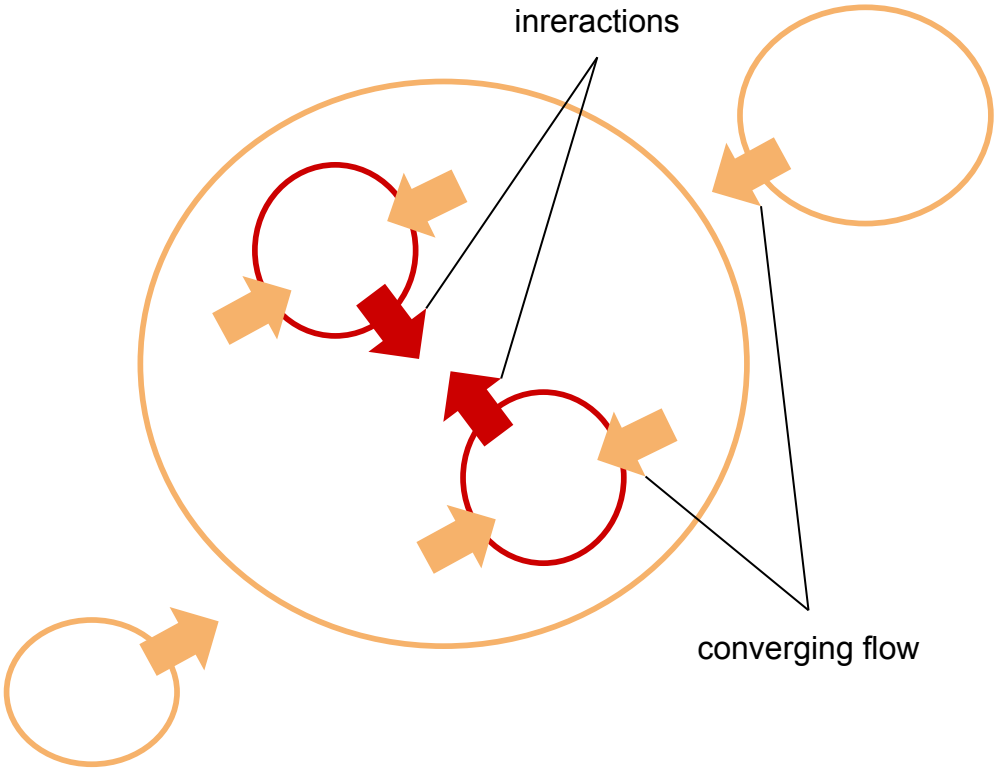

5. Discussion

Environmental dependence of YSO and massive clump formation

・YSO (low-mass star)

No significant difference in the number of internal structures was observed between leaves and isolated structures.

Low-mass star formation activity is determined solely by the properties of high-density gas, and the presence or absence of hierarchy is irrelevant.

consistent with the theory (e.g., Lada et al. 2010)

・Hi-GAL clump (high-mass star)

Leaves have a significantly higher number of inclusions.

Unlike isolated structures where gas is quickly depleted, leaves can generate numerous high-mass clumps through continuous gas supply and interaction.

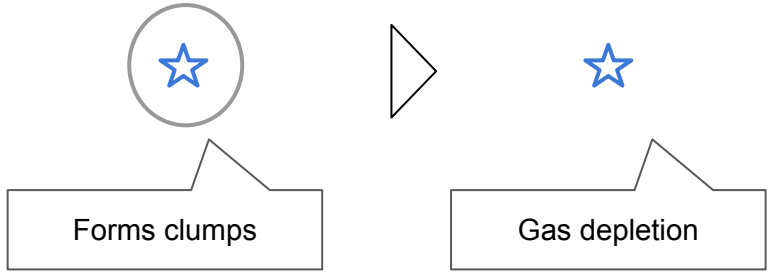

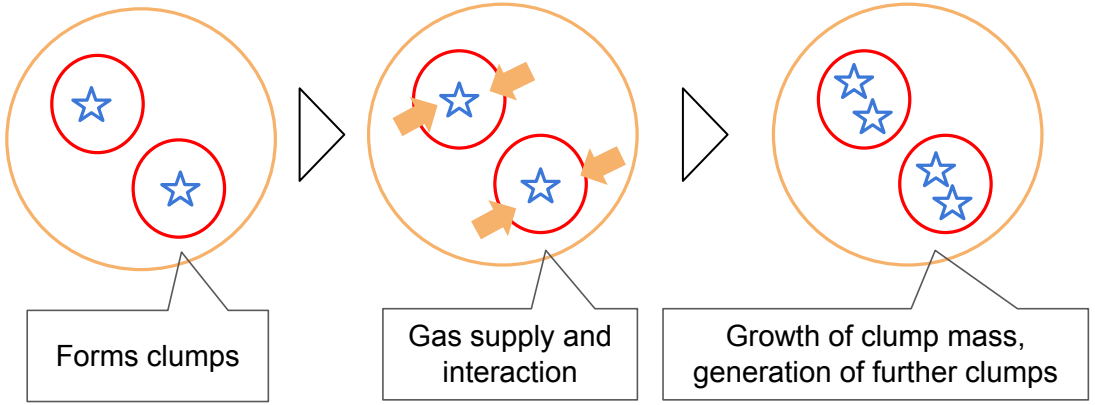

6. Summary

Work

- analyzed major Galactic star-forming regions using FUGIN data
- classified structures into hierarchical (leaf) and isolated using dendrogram

Results

- The hierarchical structure existed along the fragmented filaments, HFS, CCC bridge structures, and velocity gradients.
- Compared to isolated structures, trunks were larger in size, have higher mass.

  → **It is caused by large-scale observational phenomena and exhibits fragmentation due to strong self-gravity.**
- Compared to an isolated structure, leaves had a higher mass and density even at the same size.
- Unlike YSO, the number of clump inclusions was significantly higher in leaf structures than in isolated structures.

  → **Gas supply from the trunk and interactions allow for large-scale growth and the creation of more clumps.**

Conclusion

The trunk created by large-scale events caused by converging flows acts as a gas reservoir, promoting interactions so that the dense internal structure can continuously produce more massive stars without losing gas.

The hierarchical structure extracted by the dendrogram accurately traces the physical picture presented by the GHC scenario.

7. Future work

Observation of M33

Intragalactic observations:

lack of depth position information, inclusion of irrelevant sources...

→ **There are limitations to the accuracy of hierarchical structure analysis.**

Observation of M33:

face-on = The distribution of molecular clouds relative to the galactic plane can be accurately determined.

comparative study based on differences in galactic environments

→ **This enables more accurate and advanced discussions of hierarchical evolution.**

wide-area observation using a single mirror (trunk) + detailed observation (leaf) using interferometer

→ analysis using dendrograms

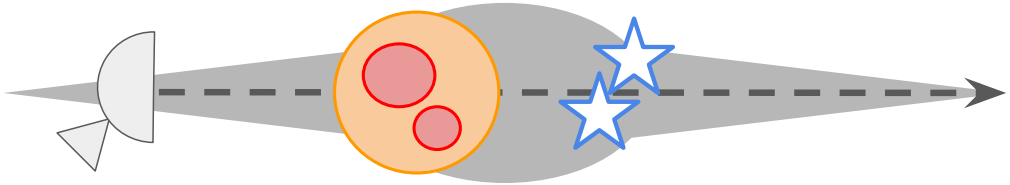

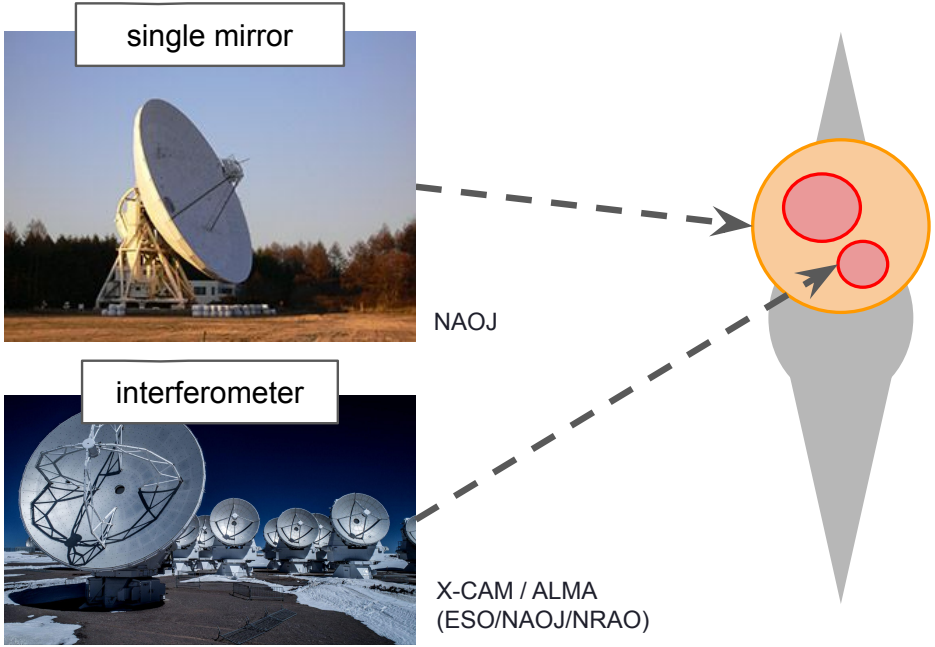

7. Future work

High-resolution fluid dynamics calculations using GPUs

Fluid dynamics calculations using GPU-accelerated code

high-resolution fluid dynamics calculations using the GPU-equipped supercomputer Miyabi (JCAHPC)

We adopted the GPU port of the self-gravitation fluid code SFUMATO (Matsumoto 2007) (Fukushima-san).

→ **Achieves speeds more than 10 times faster and higher resolution compared to conventional models.**

Direct comparison with observations

Create pseudo-observation data from calculation result data.

The data was analyzed using a dendrogram and compared with the results of the analysis of the observed data.

→ **We tracked the time evolution of the hierarchical structure and examined the validity of the scenarios obtained from observational data.**

CCS

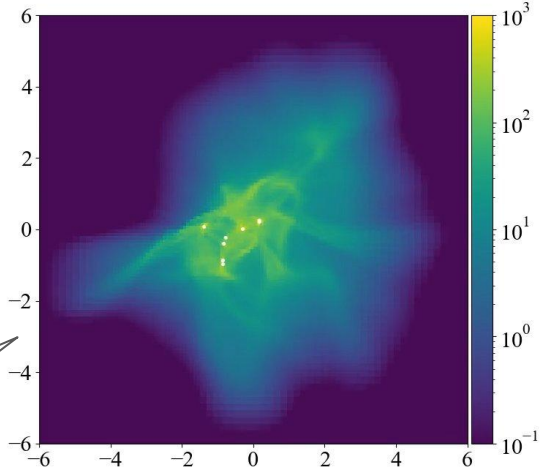

time evolution simulation of a self-gravitating fluid sphere

Appendix

List of Target Areas

Area	Galactic Longitude [degree]	Galactic Latitude [degree]	Radial Velocity [km s^{-1}]	Distance [kpc]
G18.15-0.30+51	17.8 - 18.8	-0.8 - 0.0	25 - 75	6.07
G45.3+0.1	45.0 - 45.6	-0.3 - 0.3	50 - 75	8.00
M16 (eagle nebula)	16.6 - 17.4	0.1 - 0.9	14 - 30	1.74
M17	14.8 - 15.5	-0.8 - -0.3	0 - 30	1.98
N4	11.8 - 12.0	0.7 - 1.0	20 - 30	2.80
N14	13.7 - 14.9	-0.6 - 0.1	30 - 50	3.10
N35	24.1 - 24.7	-0.1 - 0.5	100 - 130	8.80
W33	12.5 - 13.5	-0.5 - 0.5	15 - 60	2.40
W42	25.5 - 26.0	-0.5 - 0.0	85 - 125	3.80
W43	30.2 - 31.2	-0.5 - 0.5	70 - 120	5.49
W49N	42.8 - 43.4	-0.4 - 0.2	-5 - 20	11.11
W51A	48.7 - 49.7	-0.7 - 0.3	40 - 75	5.40

Appendix

Resolution Correction

Area	Distance [kpc]	Resolution [arcsec]
G18.15-0.30+51	6.07	37
G45.3+0.1	8.00	28
M16 (eagle nebula)	1.74	128
M17	1.98	112
N4	2.80	79
N14	3.10	72
N35	8.80	25
W33	2.40	93
W42	3.80	58
W43	5.49	40
W49N	11.11	20
W51A	5.40	41

Using imsmooth by CASA, the resolution is corrected according to distance and the spatial scale is unified.

Aligned with the farthest target, W49N (11.11 kpc), the corrected resolution of a target at a distance d of 1000 kpc is $20'' \times (11.11/d)$

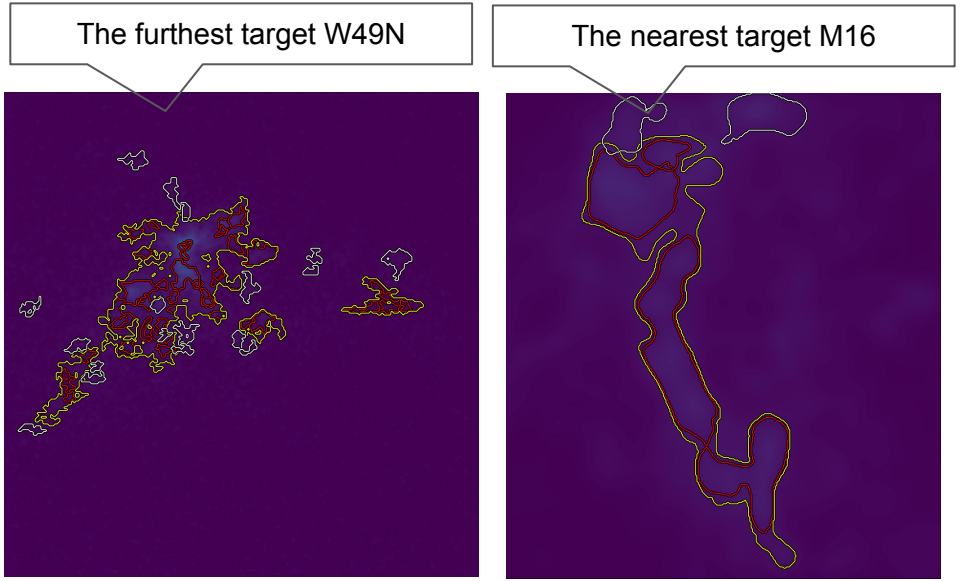

Appendix

Column Density Calculation (Excitation Temperature)

$$\begin{aligned}\Delta I_{12} &= (1 - e^{-\tau_{12}})(B_\nu(T_{\rm ex}) - B_\nu(T_{\rm bg})) \\ &= (B_\nu(T_{\rm ex}) - B_\nu(T_{\rm bg})) \qquad \because \tau_{12} \gg 1\end{aligned}$$

$$\Delta I_{12} = \frac{2k\nu_{12}^2}{c^2} T_{\rm peak} \quad B_\nu(T) = \frac{2h\nu_{12}^3}{c^2} \frac{1}{e^{h\nu_{12}/kT} - 1}$$

$$\begin{aligned}\therefore T_{\rm peak} &= \frac{h\nu_{12}}{k} \frac{1}{e^{h\nu_{12}/kT_{\rm ex}} - 1} - \frac{h\nu_{12}}{k} \frac{1}{e^{h\nu_{12}/kT_{\rm bg}} - 1} \\ &= \frac{5.53}{e^{5.53/T_{\rm ex}} - 1} - 0.819\end{aligned}$$

$$\Rightarrow T_{\rm ex} = \frac{5.53}{\ln\left(1 + \dfrac{5.53}{T_{\rm peak} + 0.819}\right)}$$

Appendix

Column Density Calculation (Optical Thickness)

$$\Delta I_{13} = (1 - e^{-\tau_{13}})(B_\nu(T_{\rm ex}) - B_\nu(T_{\rm bg}))$$

$$\Rightarrow \tau_{13} = -\ln\left(1 - \frac{\Delta I_{13}}{B_\nu(T_{\rm ex}) - B_\nu(T_{\rm bg})}\right)$$

$$\Delta I_{13} = \frac{2k\nu_{13}}{c^2} T_{\rm b}$$

$$\tau_{13} = -\ln\left(1 - \frac{T_{\rm b}}{\frac{h\nu_{13}}{k}\frac{1}{e^{h\nu_{13}/kT_{\rm ex}} - 1} - \frac{h\nu_{13}}{k}\frac{1}{e^{h\nu_{13}/kT_{\rm bg}} - 1}}\right)$$

$$= -\ln\left(1 - \frac{T_{\rm b}}{5.29(J - 0.164)}\right), \quad J = \frac{1}{e^{5.29/T_{\rm ex}} - 1}$$

Appendix

Column Density Calculation (Column Density)

$$N_{13} = \frac{3k}{8\pi^3 \mu^2 B} \frac{T_{\rm ex} + 0.88}{1 - e^{-h\nu_{13}/kT_{\rm ex}}} \int \tau_{13} dv$$

$$= 2.42 \times 10^{14} \frac{T_{\rm ex} + 0.88}{1 - e^{-5.29/T_{\rm ex}}} \int \tau_{13} dv$$

Here, partition function is $Q = \sum_J (2J+1) e^{-\frac{E_J}{kT_{\rm ex}}} \sim \frac{kT_{\rm ex}}{hB} + \frac{1}{3} \sim T_{\rm ex} + 0.88$

$$N_{\rm H_2} = 5.0 \times 10^5 N_{13}$$ （Dickman 1978）

Appendix

Details of the Type II ANOVA

$$y_{\mathrm{A}}^{\mathrm{iso}} = \mu + \epsilon_{\mathrm{A}}^{\mathrm{iso}}$$
$$y_{\mathrm{B}}^{\mathrm{iso}} = \mu + \alpha_{\mathrm{region}} + \epsilon_{\mathrm{B}}^{\mathrm{iso}}$$
$$y_{\mathrm{A}}^{\mathrm{leaf}} = \mu + \beta_{\mathrm{structure}} + \epsilon_{\mathrm{A}}^{\mathrm{leaf}}$$
$$y_{\mathrm{B}}^{\mathrm{leaf}} = \mu + \alpha_{\mathrm{region}} + \beta_{\mathrm{structure}} + \epsilon_{\mathrm{B}}^{\mathrm{leaf}}$$

$$\Rightarrow \begin{pmatrix} y_{\mathrm{A}}^{\mathrm{iso}} \\ y_{\mathrm{B}}^{\mathrm{iso}} \\ y_{\mathrm{A}}^{\mathrm{leaf}} \\ y_{\mathrm{B}}^{\mathrm{leaf}} \end{pmatrix} = \begin{pmatrix} 1 & 0 & 0 \\ 1 & 1 & 0 \\ 1 & 0 & 1 \\ 1 & 1 & 1 \end{pmatrix} \begin{pmatrix} \mu \\ \alpha_{\mathrm{region}} \\ \beta_{\mathrm{structure}} \end{pmatrix} + \begin{pmatrix} \epsilon_{\mathrm{A}}^{\mathrm{iso}} \\ \epsilon_{\mathrm{B}}^{\mathrm{iso}} \\ \epsilon_{\mathrm{A}}^{\mathrm{leaf}} \\ \epsilon_{\mathrm{B}}^{\mathrm{leaf}} \end{pmatrix}$$

$$\Rightarrow \mathbf{Y} = \mathbf{X}\boldsymbol{\theta} + \boldsymbol{\epsilon}$$

region A

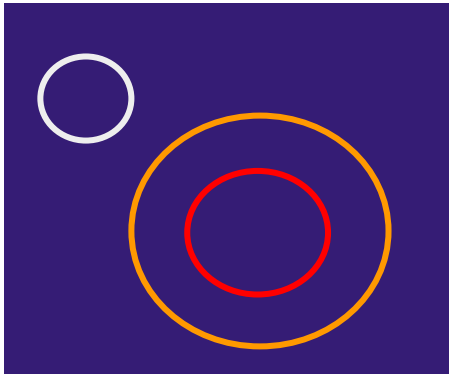

region B

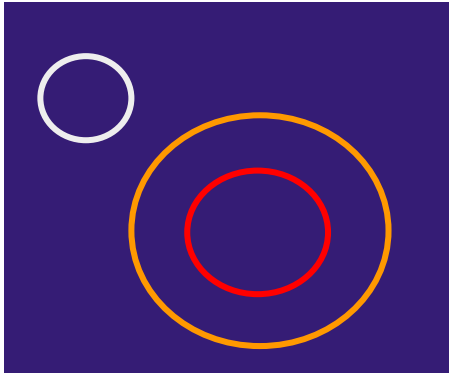

Appendix

Details of the Type II ANOVA

$$SSE_{\text{full}} = \sum \epsilon_i^j = (\mathbf{Y} - \mathbf{X}\hat{\boldsymbol{\theta}})^T(\mathbf{Y} - \mathbf{X}\hat{\boldsymbol{\theta}}) \qquad \hat{\boldsymbol{\theta}} = (\mathbf{X}^T\mathbf{X})^{-1}\mathbf{X}^T\mathbf{Y}$$

Let's assume that all structural differences are explained by ε':

$$\begin{pmatrix} y'^{\,\text{iso}}_{\text{A}} \\ y'^{\,\text{iso}}_{\text{B}} \\ y'^{\,\text{leaf}}_{\text{A}} \\ y'^{\,\text{leaf}}_{\text{B}} \end{pmatrix} = \begin{pmatrix} 1 & 0 \\ 1 & 1 \\ 1 & 0 \\ 1 & 1 \end{pmatrix} \begin{pmatrix} \mu' \\ \alpha'_{\text{region}} \end{pmatrix} + \begin{pmatrix} \epsilon'^{\,\text{iso}}_{\text{A}} \\ \epsilon'^{\,\text{iso}}_{\text{B}} \\ \epsilon'^{\,\text{leaf}}_{\text{A}} \\ \epsilon'^{\,\text{leaf}}_{\text{B}} \end{pmatrix}$$

$$SSE_{\text{reduced}} = \sum (\epsilon'^{\,j}_i)^2$$

$$SS_\beta = SSE_{\text{reduced}} - SSE_{\text{full}}$$

Appendix

Details of the Type II ANOVA

$$MS_\beta = \frac{SS_\beta}{\mathrm{df}_\beta}, \quad MS_\epsilon = \frac{SSE_{\mathrm{full}}}{\mathrm{df}_\epsilon}.$$

$$\mathrm{df}_\beta = 2 - 1 = 1$$

$$\begin{aligned} \mathrm{df}_\epsilon &= \mathrm{df}_{\mathrm{total}} - (\mathrm{df}_\alpha + \mathrm{df}_\beta) \\ &= (4 - 1) - (1 + 1) \\ &= 1 \end{aligned}$$

$$F = \frac{MS_\beta}{MS_\epsilon} \longrightarrow p$$

Appendix

Clopper-Pearson personality confidence intervals

The upper limit p_U is the value above which the probability that the inclusion rate is k/n or smaller becomes α/2.

p_Uがこれ以上高いと内包率がk/n以下である確率がα/2になってしまうという上限値p_U

$$\sum_{x=0}^{k} \binom{n}{x} p_U^x (1-p_U)^{n-x} = \frac{\alpha}{2}$$

The lower limit p_L is the value below which the probability that the inclusion rate is k/n or larger becomes α/2.

p_Lがこれ以上低いと内包率がk/n以上である確率がα/2になってしまうという下限値p_L

$$\sum_{x=k}^{n} \binom{n}{x} p_L^x (1-p_L)^{n-x} = \frac{\alpha}{2}$$